

# Requirement for and Use of Coated P92 Steel for Enhanced Structural Integrity at High Temperature

T.M. HOEY<sup>a,\*</sup>, R. CHEN<sup>a</sup>, D.G. MCCARTNEY<sup>a</sup>, W. SUN<sup>a</sup>, J. MANSFIELD<sup>b</sup>,  
P. BARNARD<sup>b</sup> AND J. FOSTER<sup>c</sup>

<sup>a</sup>Department of Mechanical, Materials and Manufacturing Engineering, Faculty of Engineering,  
University of Nottingham, Nottingham NG7 2RD, UK

<sup>b</sup>Doosan Babcock Ltd, Renfrew PA4 8DJ, UK

<sup>c</sup>Praxair Surface Technologies, Weston-super-Mare BS24 9AX, UK

To achieve climate change targets and to improve the efficiency of fossil fuel power plant the temperature and pressure of operation must be increased. With steam temperatures predicted to rise by 50–100 K in the next 30 years, this presents a number of material challenges, not least for the ferritic steels used for steam pipework. Currently the best in class ferritic steel for power plant steam pipework is P92, a 9–12% Cr advanced martensitic steel that was developed for its superior high temperature creep resistance. This paper will give a brief overview of P92 microstructure, composition and metallurgy and identify experimentally and computationally some key features of the material. As well as failure by creep, P92 at high temperature also suffers from steam oxidation damage. Recent literature suggests that coatings applied to P92 are a very promising solution. A short review of previous work on steam oxidation resistant coatings for P92 is included. A novel Co–Cr–C coating that has not previously been explored for this application is described. Experimental and computational characterisation is included.

DOI: [10.12693/APhysPolA.128.514](https://doi.org/10.12693/APhysPolA.128.514)

PACS: 81.05.Bx, 81.15.Pq, 68.37.-d, 61.05.-a, 64.75.-g

## 1. Introduction

Improving the efficiency of a coal fired power plant is strongly dependent on increase of both the temperature and pressure of operation. However as well as reduced creep life, increasing steam temperatures can cause increased steam oxidation of P92 ferritic steel, used for steam carrying pipework, leading to reduced component life.

The microstructure of P92 consists of tempered martensite with a high dislocation density and a number of finely distributed carbides, nitrides or carbo-nitrides [1]. The tempered martensite is formed during austenitisation, normalisation and finally tempering heat treatment. The main precipitates are MX (where X is C and/or N and M is V and/or Nb),  $M_{23}C_6$  (M = Cr, Mo, Fe, W) and Laves phases.  $M_{23}C_6$  carbides are normally located at grain boundaries while MX are distributed homogeneously throughout the grains.  $M_{23}C_6$  and MX particles precipitate during tempering and the Laves phase may precipitate during the service life of the component (during creep exposure or isothermal ageing) at temperatures below the final tempering temperature [2]. The microstructure of P92 has been carefully engineered to give P92 superior creep properties, for example the even distribution of precipitates can pin dislocations and the small grain size can prevent dislocation movement [3].

As mentioned, increased steam temperatures mean increased steam oxidation of P92. This oxidation causes

brittle, multi-layered, fast growing oxide scales to form that spall from the surface during ramp up and down, causing pipework damage. Typically the oxide would be formed of an inner (Cr, Fe) spinel layer and an outer magnetite layer. In some cases a haematite layer forms on top of the magnetite as a further outermost layer [4, 5]. Further alloying of P92 has been considered for protection but the formation of a detrimental, brittle Z phase is problematic as it significantly affects the mechanical performance of P92 [6].

Therefore oxidation resistant coatings [7], which form a stable and slow growing oxide as a barrier to oxidation [8], are now being considered when applied to P92. Aluminide diffusion coatings have traditionally been the focus of coated P92 research. When exposed to steam conditions a protective slow growing oxide layer,  $Al_2O_3$ , forms on the surface. However, extensive recent literature states that aluminides on P92 have a number of limitations with interdiffusion [9] and porosity forming beneath the coating [10]. This results in reduced creep strength thus limiting their service life [11]. Therefore the next generation of P92 coatings is needed.

This project considers a Co–Cr–C coating for this novel application. According to the literature [12], similar Co–Cr–C coatings have predominantly only been exploited for their oxidation resistance when applied to superalloy substrates operating at  $> 800^\circ\text{C}$ . However, the adherent oxide produced is potentially very promising for the coated P92 application and therefore needs further investigation.

\*corresponding author; e-mail: [enxtmho@nottingham.ac.uk](mailto:enxtmho@nottingham.ac.uk)

The purpose of this paper is to microstructurally characterise the P92 substrate material and the novel Co–Cr–C coating. This paper is intended as a general introduction to a novel research topic.

## 2. Experimental procedure

### 2.1. Materials

P92 (austenitised:  $\sim 1070^\circ\text{C}$  and tempered:  $\sim 775^\circ\text{C}$ ) was supplied as a pipe section, with a composition given in the Table. It was machined using wire electric discharge machining (EDM) into a number of specimens for microstructural examination.

TABLE

P92 elemental composition in wt%, determined experimentally.

Element	Weight percentage
carbon	0.10
silicon	0.19
manganese	0.46
phosphorus	0.013
sulphur	<0.002
chromium	8.72
molybdenum	0.51
nickel	0.14
aluminium	<0.02
copper	0.17
nitrogen	0.051
niobium	0.05
vanadium	0.18
tungsten	1.70
boron	0.003

The novel overlay coating is a Co–Cr–C composite coating deposited by electrodeposition onto P92 samples with a final coating thickness of 25–30  $\mu\text{m}$ . Typically the coating contains 34–40 wt% carbide ( $\text{Cr}_3\text{C}_2$ ) within a predominantly cobalt matrix. The carbides are typically irregular in shape and vary in size. The nominal composition of the coating is 66 wt% Co, 29.5 wt% Cr and 4.5 wt% C.

A number of the Co–Cr–C samples were heat treated for 6 h at  $650^\circ\text{C}$  in air to induce the formation of a surface oxide.

### 2.2. Microstructural characterisation

Uncoated and coated P92 samples were cut into optical microscopy and scanning electron microscopy (SEM) samples using a diamond cutting wheel. They were then mounted in conductive resin and polished to a 1  $\mu\text{m}$  finish on a diamond polishing wheel. Colloidal silica polishing was further used for preparation of the SEM samples. All coated samples were prepared as cross-sections so the coating-substrate interface could be examined.

For optical microscopy the samples were etched with alcoholic ferric chloride for two seconds to reveal the microstructure. For SEM some samples were examined in the unetched condition, while others were etched with

Vilella's reagent (1 g picric acid, 5 ml HCl and 100 ml alcohol) for 60 s.

Transmission electron microscopy (TEM) samples were prepared using the focused ion beam milling technique.

Energy dispersive X-ray spectroscopy (EDX) was also used and combined with SEM and TEM imaging to identify the elemental composition of phases of interest. X-ray diffraction (XRD) was also used to identify phases within the coating and on the coating surface.

ImageJ image analysis software was also used to estimate the area fraction of different phases within the coating material, the results of which are an estimate of the volume fraction of phases. The mean volume fraction from a series of measurements was then combined with known densities of phases and the composition in wt% of the coating was calculated.

### 2.3. Thermodynamic modelling

Thermo-Calc [13] is CALPHAD (CALculation of PHase Diagram) software. It allows equilibrium thermodynamics of a system to be modelled. Calculations are performed by minimising the Gibbs energies of the phases using information from empirical databases. The software was used to calculate diagrams of phase fraction against temperature for P92 and Co–Cr–C, from nominal or experimentally determined compositions. In the case of P92 the full elemental composition was used with iron being the balance element for the calculation. Thermo-Calc was also used to calculate the effect of temperature on precipitate compositions and to explore how minor compositional changes affect the constitution of P92. The TCFE7 steels database was used for P92 modelling and the SSOL5 database for Co–Cr–C modelling.

## 3. Results and discussion

### 3.1. Microstructural characterisation of P92

Optical microscopy, SEM and TEM were used to characterise the P92. Figure 1 shows the microstructure

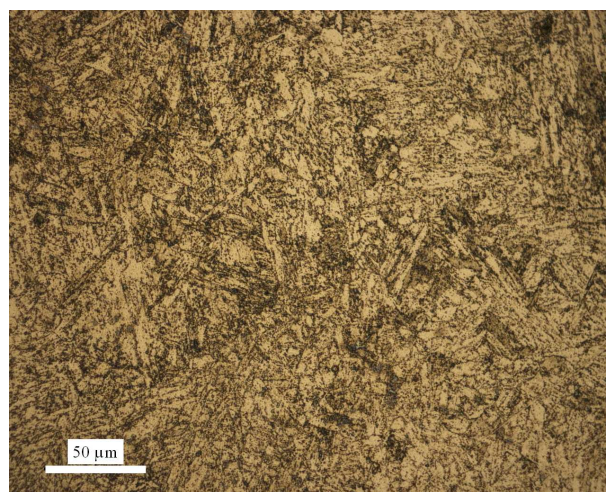


Fig. 1. Optical micrograph of the microstructure of P92, showing the tempered martensitic lath structure. Etched with alcoholic ferric chloride.

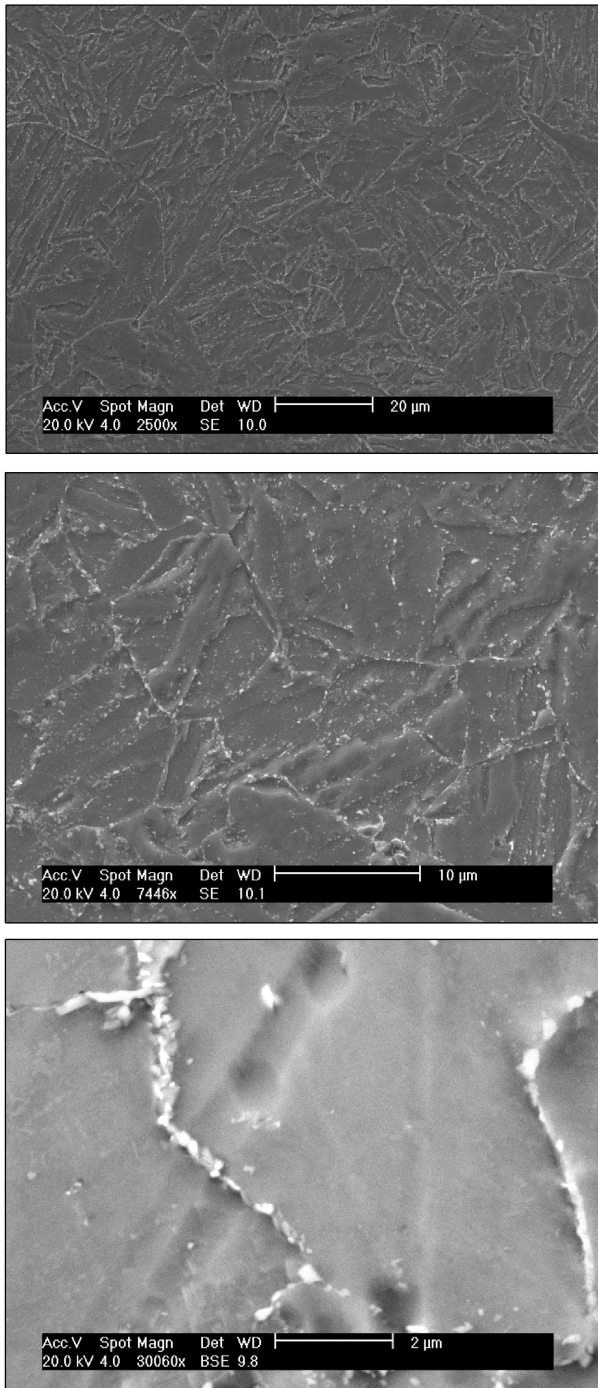


Fig. 2. SE SEM image of P92 showing: (a) the prior austenite grain boundaries and tempered martensitic lath boundaries and (b) a number of submicron precipitates located at the prior austenite grain boundaries and tempered martensitic lath boundaries. (c) High magnification BSE SEM image of P92 showing a number of submicron precipitates located along prior austenite grain boundaries and tempered martensitic lath boundaries. All etched with Vilella's reagent.

of the as received P92 steel, which consists of tempered martensitic laths.

Secondary electron (SE) SEM images in Fig. 2a and b show clearly precipitates at prior austenite grain

boundaries and tempered martensitic lath boundaries. It would appear from the backscattered electron (BSE) images in Fig. 2c that two types of precipitate are present. However, they are too small to be conclusively identified by EDX analysis. Although they could not be firmly identified, EDX analysis showed that they were enriched in Mo and W and also contained Cr. According to literature the most common precipitates are: the Laves phase,  $M_{23}C_6$  and MX [1, 2].  $M_{23}C_6$  are typically observed at prior austenite grain boundaries, sub-grain boundaries and martensitic lath boundaries. MX phase is typically observed within the grain interior. The Laves phase usually precipitates during high temperature creep or ageing. It would thus appear that the particles seen in Fig. 2 are predominantly  $M_{23}C_6$  ((Cr, Fe, Mo, W) $_{23}C_6$ ) with possibly MX phase also present, although this is usually too small to be observed by SEM.

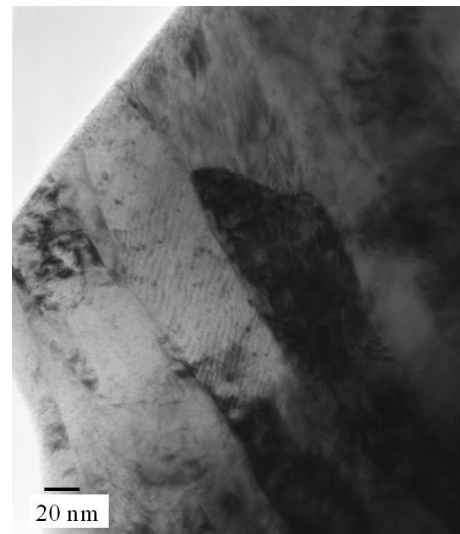


Fig. 3. TEM image of P92 showing the laths of tempered martensite.

TEM imaging also identified the distinctive lath structure in P92 as shown in Fig. 3. Although not visible in Fig. 3, sub-micron particles were found at lath boundaries that were chromium and vanadium rich according to EDX analysis. According to the literature vanadium rich particles are MX phase and chromium rich particles are  $M_{23}C_6$ .

For the P92 composition (the Table) in this study Thermo-Calc was used to produce a phase fraction diagram (Fig. 4a), in the form of phase volume fraction versus temperature, using the TCFE7 Thermo-Calc database. The main phases predicted for P92 in the temperature range 500–950 °C are: austenite (face centred cubic — fcc), ferrite (body centred cubic — bcc), MX,  $M_{23}C_6$  and Laves phase. At 650 °C (possible future service temperature) ferrite (95%), carbide and Laves phase are dominant. This agrees with previous microstructural observations and modelling work [14]. The temperature at which the ferrite to austenite transformation begins on heating is identified as 819 °C. Beyond this temperature

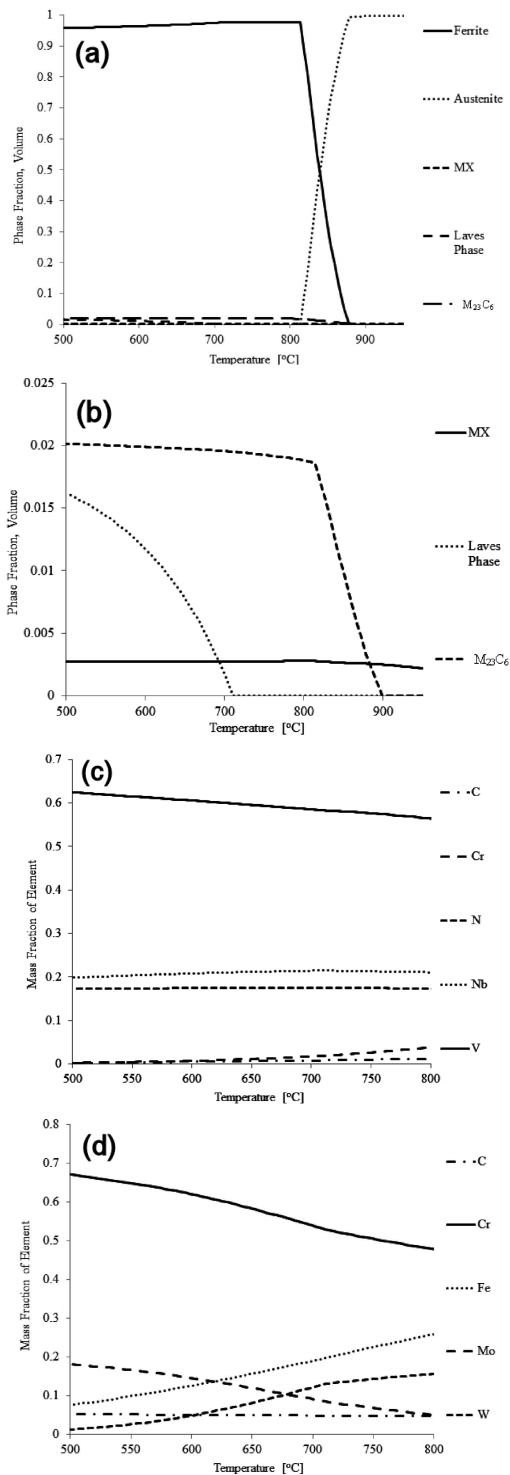


Fig. 4. (a) Phase fraction diagram for P92 steel, between 500 and 950 °C, calculated using Thermo-Calc software. Showing the ferrite to austenite transformation temperature. (b) Precipitate phase fraction diagram for P92 steel, considering 500–950 °C and up to a phase fraction of 0.025, calculated using Thermo-Calc software. Showing the change in precipitate phase fraction as temperature is increased. (c) Predicted composition of MX phase, plotted to show how the mass fraction of the elements varies with temperature. (d) As in (c), but for  $M_{23}C_6$  phase.

significant microstructural transformation occurs. Figure 4b, an enlarged section of the phase fraction diagram in Fig. 4a, also shows that as temperature is increased beyond typical operating conditions the Laves and  $M_{23}C_6$  phases begin to decrease while the MX phase remains approximately constant. Literature suggests that this evolution with temperature can detrimentally affect the creep life of P92 [3].

Thermo-Calc was also used to calculate changes in equilibrium precipitate composition with temperature. The MX phase is calculated to be rich in vanadium and/or niobium as shown in Fig. 4c. As temperature is increased, between 500 and 800 °C, there is a slight decrease in vanadium composition and an increase of the other minor elements. The  $M_{23}C_6$  phase is calculated to be rich in chromium as shown in Fig. 4d. This model also shows that  $M_{23}C_6$  shows the largest compositional change with increased temperature, the chromium content decreases whilst the iron and tungsten increase. Although not shown in this paper, the Laves phase is also calculated to be rich in tungsten, iron and molybdenum. The composition varies very slightly with temperature (increasing temperature decreases the tungsten content and increases the iron content) but overall the Laves phase composition appears stable between 500 and 800 °C.

To get an indication of how elemental variation can affect precipitation in P92 Thermo-Calc was further used to model how the phase fraction of precipitate phases in P92 vary as the weight percentage of an alloying element is varied (iron is again used to balance the composition). The temperature was chosen to be 650 °C for these calculations. Increasing the level of molybdenum in P92 by 0.3 wt% results in approximately a 40% increase in the phase fraction of the Laves phase and a less than 5% increase in the phase fraction of  $M_{23}C_6$ . The MX phase fraction remains unchanged. Increasing the level of tungsten in P92 by 0.5 wt% results in over a 100% increase in the phase fraction of the Laves phase.  $M_{23}C_6$  phase decreases by less than 1% and MX phase fraction remains unchanged. Also increasing the level of carbon in P92 by 0.06 wt% results in an increase in  $M_{23}C_6$  phase fraction by almost 90% and reduction in the Laves phase fraction by almost 30%. Nickel and silicon variation has much less effect, less than a 10% increase in the Laves phase fraction when elements increased by 0.5 wt%. These elemental variation findings are particularly relevant as it suggests that any diffusion of species (possibly entering P92 from a coating) could have a significant effect on the P92 microstructure and ultimately properties of the P92.

### 3.2. Microstructural characterisation of Co–Cr–C coating

The BSE SEM image of Fig. 5 shows the P92 substrate, labelled S, a two phase coating region, labelled C and a thin oxidised layer, labelled O.

The coating comprises dark contrast features identified by EDX and XRD as  $Cr_3C_2$  (nominally 34 wt%)

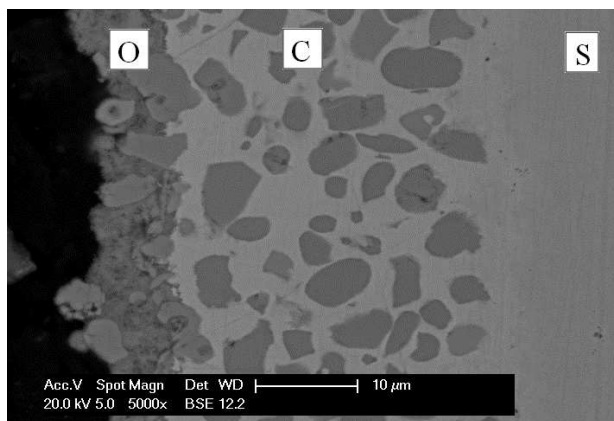


Fig. 5. A BSE SEM image of the Co-Cr-C coating applied to P92 substrate following oxidation for 6 h at 650 °C (unetched). S is the P92 substrate, C is the two-phase coating and O is the surface oxide.

and a light contrast matrix composed predominantly of cobalt. The diameter of carbides is on average measured to be 5–10  $\mu\text{m}$ , with an even distribution within the matrix.

The top surface layer is 5–10  $\mu\text{m}$  thick and appears to comprise carbides ( $\text{Cr}_3\text{C}_2$ ) and an oxide. XRD showed that the oxide layer was made up from cobalt oxide ( $\text{CoO}$  or  $\text{Co}_3\text{O}_4$ ), a spinel/mixed oxide ( $\text{CoCr}_2\text{O}_4/\text{CoO}-\text{Cr}_2\text{O}_3$ ) and chromium oxide ( $\text{Cr}_2\text{O}_3$ ).  $\text{Cr}_3\text{C}_2$  was also identified from the carbides in the surface layer. Further work is needed to clarify the spatial distribution of the different oxide phases.

Previous studies of this material suggest that the oxide will comprise the following: an outer layer of cobalt oxide or more typically a spinel or mixed oxide; and an inner layer of slow growing chromium oxide ( $\text{Cr}_2\text{O}_3$ ). The literature suggests that this oxide scale is slow-growing, adherent and dense and that the breakdown of the  $\text{Cr}_3\text{C}_2$  phase is key to the formation of the  $\text{Cr}_2\text{O}_3$  oxide and ultimately the oxidation resistance [12, 15]. This is potentially very promising for the coated P92 application.

Image analysis software combined with the known densities of  $\text{Cr}_3\text{C}_2$  was used to determine the composition in wt% of the coating, giving an overall coating composition of 62.3 wt% Co, 32.6 wt% Cr and 5.0 wt% C. This is in good agreement with the nominal stated values. These values were used with Thermo-Calc to produce a phase fraction diagram (Fig. 6). The SSOL5 database was used. Figure 6 shows that at 650 °C the equilibrium phases predicted to be present are  $\text{M}_3\text{C}_2$  ( $\text{Cr}_3\text{C}_2$  carbide), and fcc phase (cobalt matrix).

The two phase mixture appears stable between 550 and 735 °C, this includes the range of typical future service temperatures. As mentioned previously, the literature [12] suggests that the  $\text{Cr}_3\text{C}_2$  particles are available to dissolve and support formation of the double layered oxide. Thermo-Calc modelling of carbon activity in the coating and the substrate would suggest that the carbon

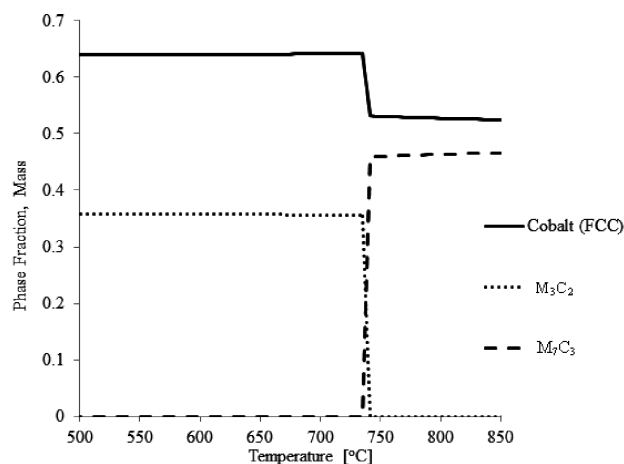


Fig. 6. Phase fraction diagram for the Co-Cr-C system, calculated using Thermo-Calc. Showing the phase fraction of fcc cobalt,  $\text{M}_3\text{C}_2$  and  $\text{M}_7\text{C}_3$  versus temperature.

from the coating might diffuse into the P92 substrate via the cobalt matrix.

It should also be noted that at 735 °C transformations of the phases are predicted to occur under equilibrium conditions, the phase fraction of the cobalt matrix begins to decrease and the carbide phase changes to  $\text{M}_7\text{C}_3$ . This predicted change requires future investigation experimentally and computationally.

#### 4. Summary

1. Experimentally P92 is shown to have a martensitic lath structure. MX and  $\text{M}_{23}\text{C}_6$  precipitates are also identified. Generally, the Laves phase would not be expected after this exposure time.
2. Thermodynamic modelling of P92 agrees with experimental characterisation and identifies: austenite (fcc), ferrite (bcc), the Laves phase, MX and  $\text{M}_{23}\text{C}_6$ . The ferrite to austenite transformation temperature, on heating, for P92 is calculated to be 819 °C.
3. At elevated temperature the phase fraction of the Laves and  $\text{M}_{23}\text{C}_6$  phases are both shown to decrease.  $\text{M}_{23}\text{C}_6$  phase is calculated to be chromium rich, MX is rich in vanadium and/or niobium and the Laves phase is rich in tungsten, iron and molybdenum. The modelling shows that temperature can significantly affect the elemental composition of precipitate phases. It is also shown that elemental variation of the minor elements in P92 has the potential to significantly alter the P92 microstructure.
4. The Co-Cr-C coating consists of chromium carbides deposited within a cobalt fcc matrix. The oxide formed consists of both cobalt and chromium oxide. The oxide is dense and adherent giving good oxidation resistance. The Co-Cr-C coating is calculated to be stable up to 735 °C.

### 5. Future work

This paper suggests that the Co–Cr–C coating is a potentially very promising solution to the problem of P92 oxidation. As such further work will be undertaken:

1. The integrity of the coating will be assessed under a number of conditions, both computationally and experimentally.
2. The interdiffusion behaviour between the coating and substrate will be considered, computationally and experimentally.
3. The effect of the coating on mechanical properties of the substrate will be considered, experimentally and computationally.

### Acknowledgments

The authors would like to thank the Research Councils UK (RCUK) and the Biomass and Fossil Fuel Research Alliance (BF2RA) for financial support. The funding is provided through the Efficient Fossil Energy Technologies Engineering Doctorate Centre based at the University of Nottingham, UK. Thanks also to Doosan Babcock Ltd and Praxair Surface Technologies for materials provided and technical support.

### References

- [1] A. Czyska-Filemonowicz, A. Ziellinska-Lipiec, P.J. Ennis, *J. Achiev. Mater. Manufact. Eng.* **19**, 43 (2006).
- [2] A. Gustafson, M. Hattestrand, *Mater. Sci. Eng. A* **333**, 279 (2002).
- [3] J.C. Vaillant, B. Vandenberghe, B. Hahn, H. Heuser, C. Jochum, *Int. J. Pres. Ves. Pip.* **85**, 38 (2008).
- [4] A.T. Fry, I.G. Wright, N.J. Simms, B. McGhee, G.R. Holcomb, *Mater. High. Temp.* **30**, 261 (2014).
- [5] M. Lukaszewicz, N.J. Simms, T. Dudziak, J.R. Nicholls, *Mater. High. Temp.* **29**, 210 (2014).
- [6] M. Yoshizawa, M. Igarashi, K. Moriguchi, A. Iseda, H.G. Armaki, K. Maruyama, *Mater. Sci. Eng. A* **510–511**, 162 (2009).
- [7] J.R. Nicholls, *JOM* **52**, 28 (2000).
- [8] M. Scheefer, R. Knödler, B. Scarlin, A.A. Bruna, D.N. Tsipas, *Mater. Corros.* **56**, 907 (2005).
- [9] R.N. Durham, L. Singheiser, W.J. Quadackers, *Mater. Corros.* **59**, 402 (2008).
- [10] E. N'Dah, S. Tsipas, M.P. Hierro, F.J. Pérez, *Corros. Sci.* **49**, 3850 (2007).
- [11] A. Aguero, R. Muelas, M. Gutiérrez, R. Van Vulpen, S. Osgerby, J.P. Banks, *Surf. Coat. Technol.* **201**, 6253 (2007).
- [12] B.P. Cameron, J. Foster, J.A. Carew, *T. I. Met. Finish.* **57**, 113 (1979).
- [13] J.O. Andersson, T. Helander, L. Höglund, P. Shi, B. Sundman, *Calphad* **26**, 273 (2002).
- [14] K. Chalk, Ph.D. Thesis, University of Nottingham, Nottingham UK 2013.
- [15] M.E. El Dahshan, J. Stringer, D.P. Whittle, *Cobalt* **3**, 86 (1974).